Molecular Modeling of Low-Emissivity Materials

S. Schweizer[*], J. J. Low[**] and L. Subramanian[*]

[*]Scienomics, 5555 Glenridge Connector, Suite 200 – Highlands One, Atlanta, GA 30342, USA, lalitha.subramanian@scienomics.com
[**]Argonne National Laboratory, 9700 South Cass Avenue Argonne, IL 60439, USA, jlow@mcs.anl.gov

ABSTRACT

Emissivity plays a critical role in energy engineering and thermal management. Using low-emissivity coatings and materials is regarded as a promising and efficient strategy to reduce the heat loss of buildings or solar collectors. In this way, the energy efficiency can be improved and costs can be saved.

Over the past years, computational methods and molecular modeling have become versatile tools to support and guide experimental developments. Predicting material properties and simulating processes at the atomistic level can provide critical insights for improving material performance and developing novel materials.

Here, we will present density functional theory (DFT) calculations on low-emissivity materials. It will be shown how simulations can be used to efficiently screen these materials and characterize their properties.

Keywords: low-emissivity, glass coating, functional building materials, density functional theory, molecular modeling

1 INTRODUCTION

Reducing heat transfer through thermal radiation is of main importance for energy efficient building. The emissivity of a material plays a central role in this context. Using low-emissivity (low-e) building materials is a very efficient way to save energy and thus costs [1]. Especially glazings and windows are quite prominent candidates for improving the energy efficiency of buildings. Low-e glass can significantly affect heating, cooling and also lighting costs [2].

Reflective insulation can, however, also be exploited for light-tight/opaque areas of a building [1], for example by incorporating low-e foils in the house envelope or using low-e materials for advanced insulating attic systems. The importance of low-e materials is not limited to buildings, but plays also a role where insulating against temperature differences is crucial. Reducing the weight of packaging for shipping temperature sensitive goods or insulating operating equipments like pipes or storage tanks can be achieved by employing low-e materials [3]. Critical aspects of low-e coatings are reducing production costs by using equally-performing cheaper materials, increasing the visible transmittance on transparent materials, the design of controllable and adaptive coatings and the long-term durability [1,4,5].

Molecular modeling is a versatile tool for improving material performance and developing novel materials. Predicting material properties using computational methods can efficiently and cost-effectively support and guide experimentation. We will present density functional theory (DFT) calculations on low-e materials. The frequency-dependent dielectric function, which can be transformed into the emissivity, has been calculated for several metal oxides that are used in low-e coatings.

2 RESULTS AND DISCUSSION

Advanced glazing coatings typically consist of one or more layer stacks [2,6,7]. The composition of a typical stack is illustrated in Figure 1.

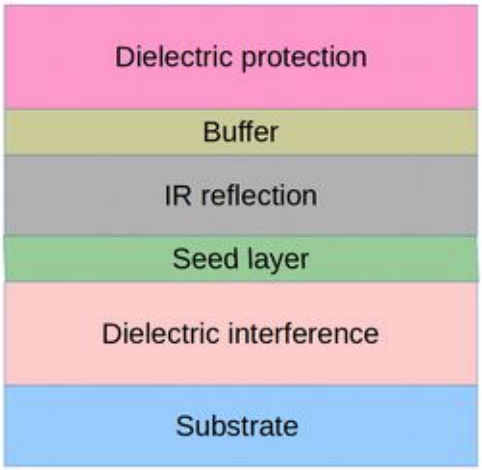

Figure 1: Layer stacking of low-e coating.

In state-of-the-art coatings, a high IR reflectance is achieved by using silver (Ag). While base and top layers govern the visible optical performance, seed and barrier layers are critical for the emissivity [2]. For the latter, metal oxides like ZnO, SnO_2, or TiO_2 are used [8]. In the following, we will present DFT simulations of the properties of ZnO, SnO_2 and MgO. MgO has been chosen because of its better lattice matching with Ag, which is a critical point from manufacturing point of view.

The unit cells of the oxides and of Ag are shown in Figure 2.

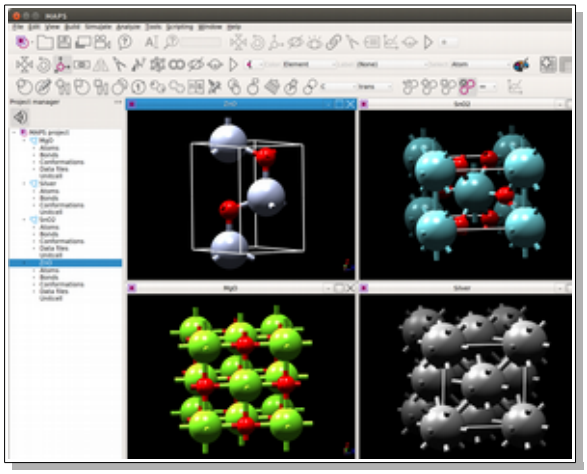

Figure 2: MAPS interface showing unit cells of ZnO (top left), SnO_2 (top right), MgO (bottom left) and Ag (bottom right).

2.1 Comparison of Pseudopotentials

For ZnO and Ag, systematic convergence studies have been performed within the generalized gradient approximation (GGA). Three sets of pseudopotentials have been used: (i) Norm-conserving PBE pseudopotentials [9], (ii) optimized norm-conserving PBE pseudopotentials [10,11], and (iii) optimized norm-conserving PBESOL pseudopotentials [12]. More details are provided in the Computational Details sections.

The convergence of the absolute energies with respect to the energy cutoff and the k-point grid has been systematically studied. For Ag, the convergence for the smearing factor has also been checked. For converging the absolute energy with the energy cutoff, the latter as been increased from 30 Ry to 400 Ry, while applying a k-point grid of 2x2x2. For all three sets of pseudopotentials, the absolute energies converged smoothly and did not change by more than $3*10^{-6}$ H for energy cutoffs higher than 300 Ry. Relative energies referring to the energy obtained for an energy cutoff of 400 Ry were calculated to assess the convergence in terms of chemical and spectroscopic accuracy which is typically regarded to be about 4 and 1 kJ/mol, respectively. For ZnO, energy differences smaller than 1 kJ/mol were obtained for the following cutoffs: 150 Ry for norm-conserving PBE pseudopotentials of set (i), 110 Ry for optimized norm-conserving PBE pseudopotentials of set (ii), and 80 Ry for optimized norm-conserving PBESOL pseudopotentials of set (iii). For Ag, the following cutoffs were found: For set (i) 80 Ry, for set (ii) 60 Ry, and for set (iii) 80 Ry.

The corresponding energy cutoffs were used to converge the k-point grid. The k-point grid was increased from 2x2x2 to 20x20x20. Relative energies smaller than 1 kJ/mol were obtained for all pseudopotentials sets with a k-point grid of 6x6x6 for ZnO and 10x10x10 or Ag. For Ag, a smearing factor of 0.005 Ry was found to provide an accuracy better than 1 kJ/mol in relative energies for pseudopotential set (iii).

Cell parameters of the geometry optimized structures of ZnO are compared for the different pseudopotential sets in Table 1.

Cell parameter	(i)	(ii)	(iii)	Experiment
a /Å	3.31	3.28	3.24	3.25
c /Å	5.34	5.29	5.19	5.20

Table 1: Cell parameter of geometry optimized structure of ZnO using different sets of pseudopotentials (for details, please see main text and Computational Details).

Cell parameters are somewhat overestimated using norm-conserving and optimized norm-conserving pseudopotentials of set (i) and (ii), while cell parameters obtained with PBESOL pseudopotentials are slightly underestimated, but showing the best agreement with the experimental data [13].

Overall, the optimized norm-conserving PBESOL pseudopotentials, i. e. set (iii), showed the fastest convergence behavior and the best agreement with experimental structural properties. Therefore, calculations for MgO and SnO_2 and property calculations were performed using pseudopotential set (iii). Convergence studies for MgO and SnO_2 were performed in a similar way as for ZnO. An energy cutoff of 80 Ry and a k-point grid of 6x6x6 were found to provide accuracies in relative energies better than 1 kJ/mol.

2.2 Frequency Dependent Dielectric Function

For all oxide structures, the frequency dependent dielectric function has been calculated using the energy cutoffs and k-point grids as found in the preliminary studies. The k-point grid has then been systematically increased to study and ensure convergence of the calculated property with the number of k-points.

For ZnO, the dielectric constant values $\varepsilon(0)_{xx}$ and $\varepsilon(0)_{zz}$ with increasing number of k-points are listed in Table 2.

k-points	$\varepsilon(0)_{xx}$	$\varepsilon(0)_{zz}$
6x6x6	13.25	10.61
8x8x8	9.84	8.38
10x10x10	8.72	7.78
12x12x12	8.24	7.58
14x14x14	8.03	7.52
16x16x16	7.91	7.49

Table 2: Dielectric constant values $\varepsilon(0)_{xx}$ and $\varepsilon(0)_{zz}$ of ZnO.

The converged values are in nice agreement with experimental results [13]. The frequency dependent dielectric function obtained using a 14x14x14 k-point grid is shown in Figure 3.

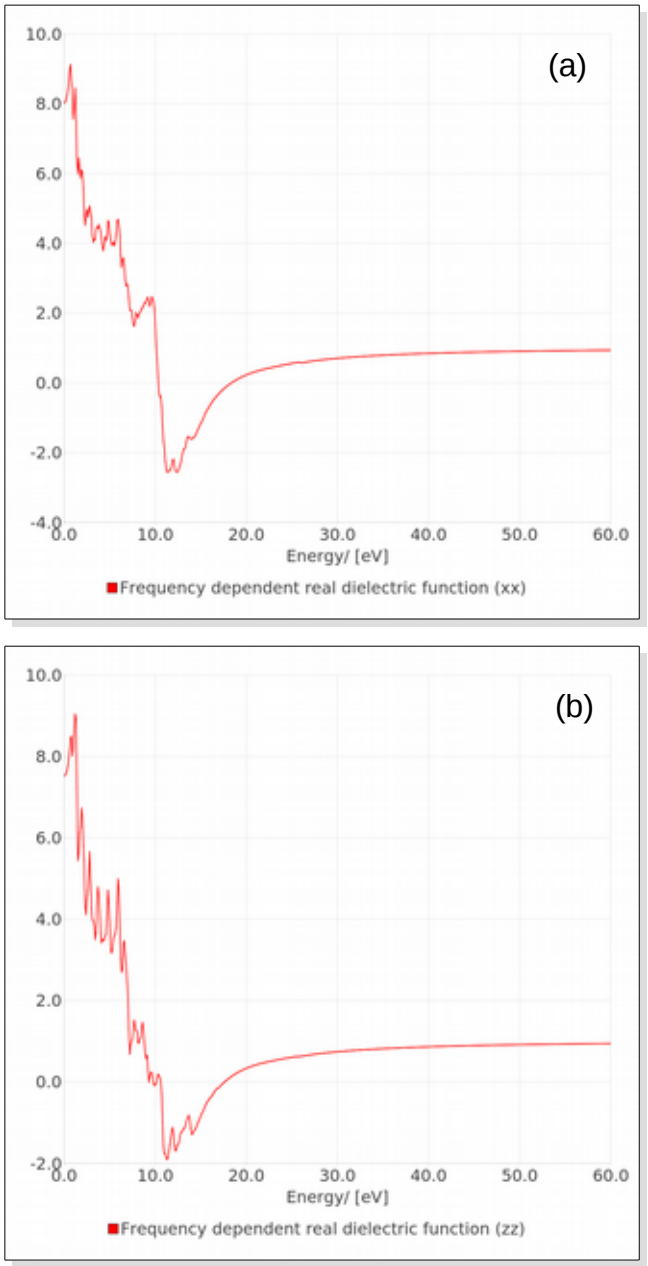

Figure 3: Frequency dependent dielectric function of ZnO. Figure 3 (a) shows xx and (b) zz.

Analogously, simulations were performed for SnO_2 and MgO. We found that the dielectric properties converged faster with the k-point grid compared to ZnO. In both cases, a grid of 8x8x8 was sufficient. For MgO, $\varepsilon(0)_{xx} = \varepsilon(0)_{zz} = 4.13$ was obtained and for SnO_2, $\varepsilon(0)_{xx} = 5.11$ and $\varepsilon(0)_{zz} = 4.97$. For MgO, $\varepsilon(0)_{xx}$ was slightly underestimated compared to experimental data [14], while for SnO_2, both values are within the experimental range [15].

3 COMPUTATIONAL DETAILS

Scienomics MAPS software platform [9] has been used (a) to create initial structures using MAPS' structure library and interface to the Crystallography Open Database, (b) to set up setup density functional theory (DFT) calculations using MAPS QuantumEspresso [16] interface and (c) to analyze the DFT simulations.

For all structures convergence studies with respect to the energy cutoff and the k-point grid have been performed. The converged values for the energy cutoff and the k-point grid have been used to geometry optimize the crystal structures stepwise. First, the atomic position have been relaxed and afterwards the whole cell. For the geometry optimized structures, the frequency-dependent dielectric function was calculated. For the latter, the convergence with the k-point grid has been evaluated for each structure.

The DFT calculations were performed applying the generalized gradient approximation. Three types of pseudopotentials have been used for convergence studies of ZnO and Ag: (i) Norm-conserving PBE pseudopotentials of the Troullier-Martins type shipped with MAPS [9], (ii) SG15 optimized norm-conserving Vanderbilt PBE pseudopotentials [10,11], and (iii) ONCVPSP PBESOL pseudopotentials from PseudoDojo [12]. For SnO_2 and MgO simulations were performed with ONCVPSP pseudopotentials only. For Ag, Fermi-Dirac smearing was used.

4 CONCLUSION

In the present work, we have shown how optical properties of metal oxides that are relevant as low-emissivity coatings can be calculated using density functional theory methods. In this context, we have compared the performance of three different sets of commonly used pseudopotentials. ONCVPSP PBESOL pseudopotentials were found to provide accurate results and showed a fast convergence behavior. Based on the results obtained in the present study, future work will focus on predicting and screening properties of oxide/silver interfaces which are of main importance for low-e coatings.

5 ACKNOWLEDGMENT

The authors gratefully acknowledge the computing resources provided on Blues and Fusion, high-performance computing cluster operated by the Laboratory Computing Resource Center at Argonne National Laboratory. L. S. would like to thank Raymond Bair at Argonne National Lab for providing HPC resources for this work.

REFERENCES

[1] B. P. Jelle, S. E. Kalnæsa, T. Gao, Energy and Buildings (2015) 96(1):329-356.

[2] G. Ding and C. Clavero, Silver-Based Low-Emissivity Coating Technology for Energy- Saving Window Applications, Modern Technologies for Creating the Thin-film Systems and Coatings, Prof. N. Nikitenkov (Ed.), InTech, 2017, DOI: 10.5772/67085.

[3] http://www.sigmalabs.com/blog/surface-emissivity-why-it-matters-in-insulation.html (accessed Dec 05, 2017).

[4] G. Leftheriotis and P. Yianoulis, Materials & Solar Cells (1999) 58:185-197.

[5] B. P. Jelle, Solar Energy Materials and Solar Cells (2013) 116:291-323.

[6] J. Mohelnikova, *7 - Nanocoatings for architectural glass*, In Woodhead Publishing Series in Metals and Surface Engineering, Woodhead Publishing, 2011, 182-202, Nanocoatings and Ultra-Thin Films.

[7] J. Finley, PPG Industries, Inc. *The future high performance Glazing in commercial buildings*, 2008, Available from: http://www.lehigh.edu/imi/teched/SolarWS/T6f_Finley.pdf.

[8] D. Cornil, H. Wiame, B. Lecomte, J. Cornil, and D. Beljonne, ACS Applied Materials & Interfaces (2017) 9(21):18346-18354.

[9] Scienomics, MAPS version 4.0.1, 2017, www.scienomics.com.

[10] D. R. Hamann, Phys. Rev. B (2013) 88:085117.

[11] M. Schlipf and F. Gygi, Computer Physics Communications (2015) 196:36-44.

[12] M. J. van Setten, M. Giantomassi, E. Bousquet, M. J. Verstraete, D. R. Hamann, X. Gonze, G.-M. Rignanese, Computer Physics Communications 2018 in press, DOI: 10.1016/j.cpc.2018.01.012.

[13] Collaboration: Authors and editors of the volumes III/17B-22A-41B () Zinc oxide (ZnO) dielectric constants. In: Madelung O., Rössler U., Schulz M. (eds) II-VI and I-VII Compounds; Semimagnetic Compounds. Landolt-Börnstein - Group III Condensed Matter (Numerical Data and Functional Relationships in Science and Technology), vol 41B. Springer, Berlin, Heidelberg.

[14] Collaboration: Authors and editors of the volumes III/17B-22A-41B () Magnesium oxide (MgO) dielectric constants, optical and photoelectric properties. In: Madelung O., Rössler U., Schulz M. (eds) II-VI and I-VII Compounds; Semimagnetic Compounds. Landolt-Börnstein - Group III Condensed Matter (Numerical Data and Functional Relationships in Science and Technology), vol 41B. Springer, Berlin, Heidelberg.

[15] Collaboration: Authors and editors of the volumes III/17E-17F-41C () Tin dioxide (SnO2) optical properties, dielectric constants. In: Madelung O., Rössler U., Schulz M. (eds) Non-Tetrahedrally Bonded Elements and Binary Compounds I. Landolt-Börnstein - Group III Condensed Matter (Numerical Data and Functional Relationships in Science and Technology), vol 41C. Springer, Berlin, Heidelberg.

[16] P. Giannozzi et al. J.Phys.:Condens.Matter (2009) 21(39):395502.